



NEW ZEALAND SOCIETY FOR EARTHQUAKE ENGINEERING  
**2019 Pacific Conference on  
Earthquake Engineering**  
TURNING HAZARD AWARENESS INTO RISK MITIGATION  
4 – 6 April | SkyCity, Auckland | New Zealand



---

# Dynamic characteristics of a six-storey wooden building based on strong motion data

*T. Kashima & H. Nakagawa*

Building Research Institute, Tsukuba, Japan.

## ABSTRACT

The Building Research Institute and the Japan 2x4 Home Builders Association jointly built a full-scale six-story wooden experimental building. The building was densely equipped with two types of accelerometers to investigate its dynamic characteristics in detail.

First, fundamental dynamic characteristics of the building considering the soil-structure interaction effect were discussed using a set of strong motion data. Natural vibration mode shapes were estimated by waveform analysis.

The seasonal fluctuation in the dynamic characteristics was recognised by the system identification using ambient vibration data. The fluctuation can be explained as the influence of temperature and relative humidity.

The fundamental natural frequencies and damping ratios were identified using the strong motion data from more than 100 earthquakes. The dependence of the dynamic characteristics on response amplitude could be observed in the analytical result.

## 1 INTRODUCTION

In Japan blessed with forest resources, many houses are made of wood. However, the Building Standards Law of Japan sets up regulations for large-scale wooden buildings from the aspects of fire protection and earthquake disaster prevention. In recent years, the use of wood for house construction has been promoted from the viewpoint of environmental protection. It requires verification of the technology developed for large-scale wooden buildings.

Against such a background, the Building Research Institute (BRI) and the Japan 2x4 Home Builders Association jointly built a full-scale six-storey wooden experimental building in the site of BRI in Tsukuba,

Japan. Various physical quantities, such as temperature and relative humidity, condensation, sound insulation, and vertical shrinkage, are being monitored in the building. As a part of the monitoring system, we installed strong motion instruments to investigate the dynamic behaviour of the building. The paper discusses dynamic characteristics of the experimental building based on the analysis of strong motion data.

## 2 OUTLINE OF THE EXPERIMENTAL PROJECT

### 2.1 Building structure

The experimental building has a wooden framing structure with a building area of 38.95 m<sup>2</sup>, a total floor area of 206.09 m<sup>2</sup>, and an eaves height of 16.91 m (Tsujimura 2016). The building is supported by eleven steel piles, each being 12 m in length. The floor plan and cross section of the building are illustrated in Figure 1.

The building does not have interior finishing and live loads. Therefore, to substitute for the weight of finishing and live loads, two or one big water pool was placed on each floor during the period from December 2016 to October 2017. Two water pools were placed on each of the second to fifth floors, and one water pool on the sixth floor. The dimensions of the water pool are 2.6 m long by 1.6 m wide, and each pool was filled with water to a depth of 0.56 m. Consequently, the masses of the individual floors were increased by 14% to 26% by adding one or two pools, each having nearly 2330 kg of mass.

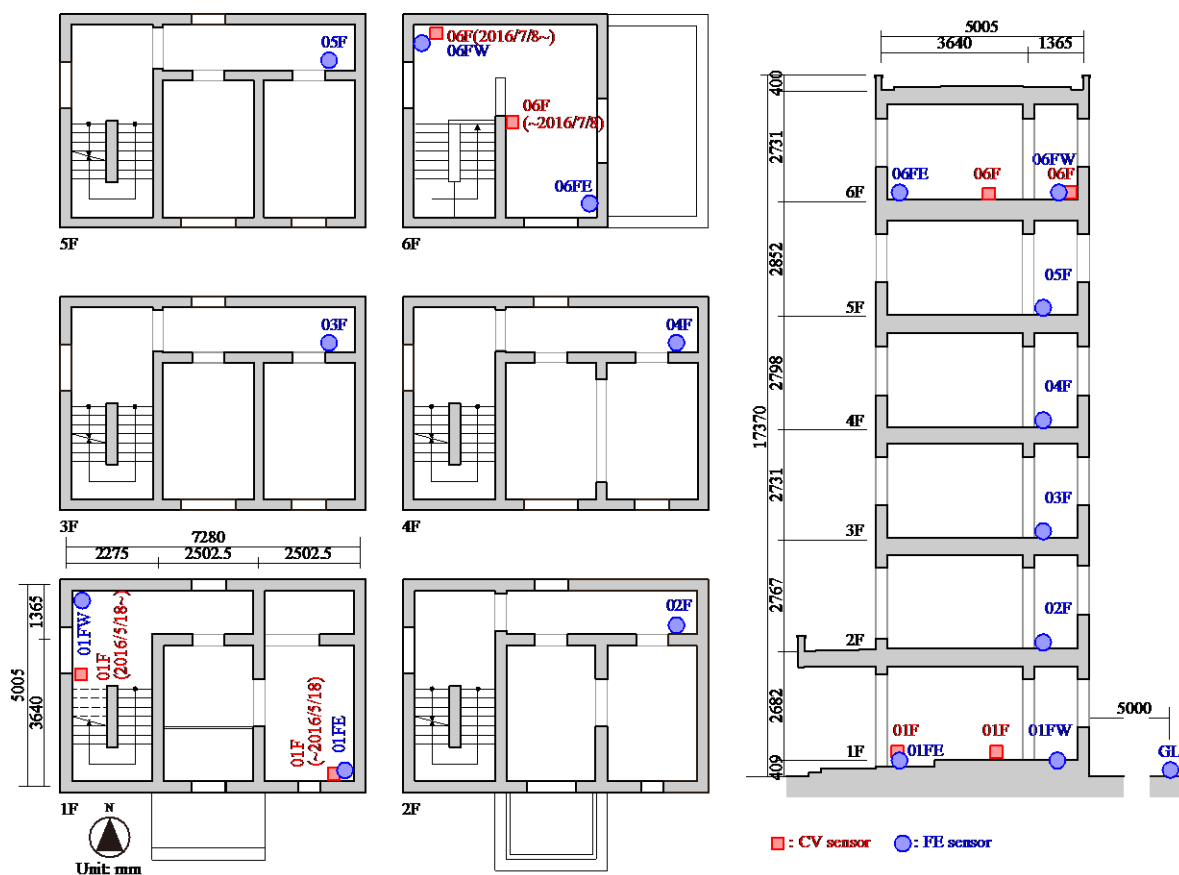


Figure 1: Floor and cross section plans, and sensor configuration

### 2.2 Strong motion instrumentation

Strong motion observation for this experimental building started in April 2016 using two types of instruments. One is a high-performance type equipped with a tri-axial force-balanced accelerometer, referred to as CV in this paper. Several CV sensors are individually working, and each instrument keeps the accurate time with calibration using GPS. The other is an economical type equipped with a tri-axial MEMS (Micro

Electronic Mechanical Systems) accelerometer, referred to as FE. A laptop PC set up on the second floor acquires acceleration data from all the FE sensors via a local area network. The clock on the PC is calibrated by NTP. The specifications of both types of instruments are listed in Table 1.

The sensor configuration in the building is plotted in Figure 1. Red squares (■) and blue circles (●) indicate CV and FE sensors, respectively. In addition to the sensors in the building, one FE sensor was set up on the ground at a distance of 5 m from the outer wall of the building. This paper discusses the dynamic characteristics of the building based on acceleration data recorded by both types of sensors.

Table 1: Specifications of strong motion instruments.

Abbr.	Product	Sensor type	Full scale	Resolution	Frequency range
CV	CV-374, Tokyo Sokushin Co., Ltd.	Force-balanced accelerometer	20 m/s <sup>2</sup>	0.00001 m/s <sup>2</sup>	DC to 100 Hz
FE	Kanshin Sensor, Fuji Electric Co., Ltd.	MEMS accelerometer	15 m/s <sup>2</sup>	0.0002 m/s <sup>2</sup>	0.1 Hz to 50 Hz

### 3 FUNDAMENTAL DYNAMIC CHARACTERISTICS OF THE BUILDING

#### 3.1 Strong motion data

In order to discuss the fundamental dynamic characteristics of the experimental building, a set of strong motion data with moderate amplitude level is selected. The earthquake with a JMA (Japan Meteorological Agency) magnitude of 7.4 and a focal depth of 25 km occurred on 22nd November 2016. Maximum accelerations recorded on each floor by the FE sensors are listed in Table 2. The maximum accelerations on the first floor were nearly 0.4 m/s<sup>2</sup> in both the horizontal directions, while those on the sixth floor were amplified more than 3.5 times and exceeded 1.4 m/s<sup>2</sup>.

Table 2: Peak accelerations of strong motion data used for analysis.

Place	Peak acc. (m/s <sup>2</sup> )		
	NS	EW	UD
GL	0.395	0.354	0.194
1F	0.387	0.392	0.175
2F	0.424	0.415	0.230
3F	0.543	0.520	0.255
4F	0.781	0.767	0.294
5F	1.110	0.987	0.306
6F	1.497	1.414	0.354

#### 3.2 Soil-structure interaction effect

The soil-structure interaction is often discussed using a simplified model having springs and dampers representing swaying (horizontal translation) and rocking (rotation) between the ground and foundation as shown in Figure 2. In this model, strong motion data at five points,  $x_G$ ,  $x_F$ ,  $x_T$ ,  $z_L$  and  $z_R$ , enable to separate the total displacement at the top floor into those caused by swaying ( $u_S$ ), rocking ( $u_R$ ), and building deformation ( $u_B$ ).

The transfer function of motions  $x_T$  to  $x_G$  ( $x_T/x_G$ ) indicates response characteristics of the system including the swaying and rocking effect, and  $x_T/x_F$  that including the rocking effect. The transfer function of  $x_F/x_G$  reflects

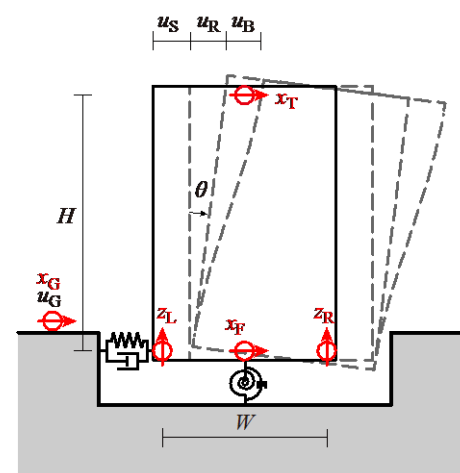


Figure 2: Swaying-rocking model.

the effect of the kinematic interaction. Those transfer functions of the strong motion are shown in Figure 3.

Comparing transfer functions of  $x_T/x_G$  and  $x_T/x_F$ , small difference can be found although the shapes are complicated. Looking at the amplitude and phase of the transfer functions in the NS direction, the natural frequency of the system including swaying and rocking can be estimated as 3.02 Hz. The system including rocking will have the natural frequency of 3.36 Hz. On the other hand, the natural frequencies with swaying and rocking and with rocking in the EW direction are 3.22 Hz and 3.64 Hz, respectively. The transfer functions of  $x_F/x_G$  in both the directions generally show flat shape in the amplitude and small values in the phase, therefore it can be said that difference between strong motions on the ground and building foundation is small.

Using the strong motion data recorded by the FE sensors, fundamental vibration mode shapes considering the soil-structure interaction are examined. The mode shapes are determined from peak values of band-pass filtered relative displacements of each floor to the ground in both the horizontal directions. Passbands for NS and EW directions are 2.8 Hz to 3.6 Hz and 3.0 Hz to 4.0 Hz, respectively.

The normalised mode shapes are shown in Figure 4. The upper and lower plots correspond to the NS and EW directions, respectively. Grey circles indicate normalised mode shape at each cycle, and solid red lines represent the average of those. Dash-dotted and dotted lines represent the swaying and rocking components, respectively. The ratios of the swaying and rocking displacements to the total top displacement in the NS component are about 7% and 25 %, respectively. Those in the EW direction are about 7% and 18%. Since the NS direction corresponds to the short side direction of the building, the effect of rocking is higher than that in the EW direction.

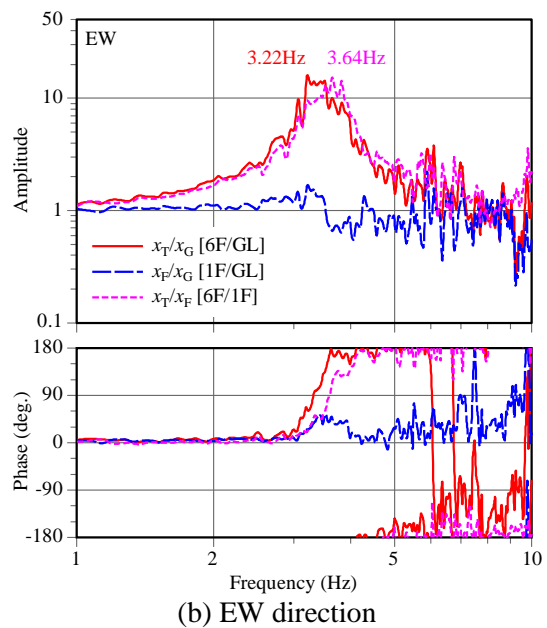
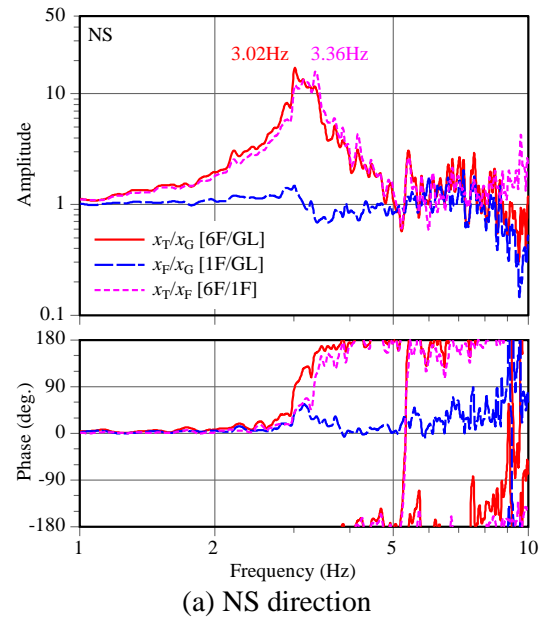
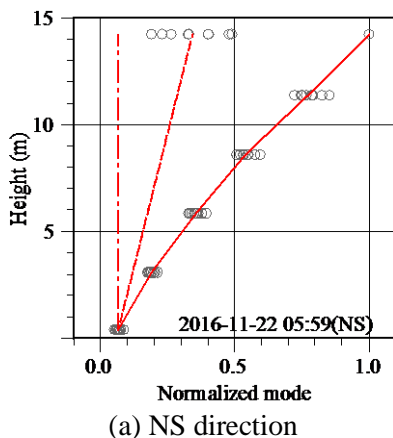


Figure 3: Transfer functions of  $x_T/x_G$ ,  $x_F/x_G$  and  $x_T/x_B$

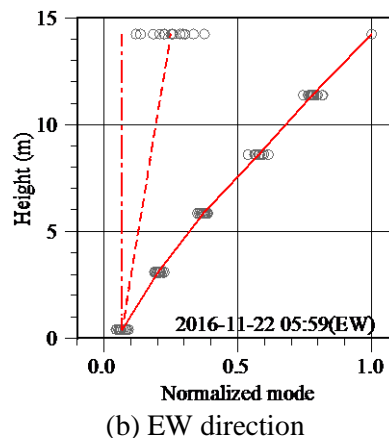


Figure 4: Vibration mode shapes considering soil-structure interaction.

## 4 SEASONAL FLUCTUATION IN DYNAMIC CHARACTERISTICS

### 4.1 Identification of daily dynamic characteristics

In order to estimate daily dynamic characteristics, which eliminate the influence of the dependence on amplitude, the natural frequencies and damping ratios were identified from ambient vibration data recorded from 00:00 to 00:10 every day. The CV sensors are continuously recording accelerations all the time. Such data can be used as ambient vibration data. The natural frequencies and damping ratios of the building were identified from ambient vibration data using the random decrement (RD) technique (Tamura et al. 1993).

The upper and lower plots in Figure 5 represent the identified natural frequencies and damping ratios, respectively. Red hollow circles ( $\circ$ ) and blue hollow triangles ( $\triangle$ ) correspond to the NS and EW directions, respectively. The grey zones indicate the period with the loading of the water pools added. Looking at the natural frequencies, seasonal fluctuation appears in both the NS and EW directions. Comparing between the natural frequencies in the winter and summer, the values in the winter are 7 % to 8 % lower than those in the summer. The damping ratios in the EW direction widely vary in the period with the additional loading (grey zone) caused by the effect of sloshing (Kashima et al. 2018).

### 4.2 Influence of weather

Weather can be a factor for such seasonal fluctuation. Figure 6 shows changes in daily averages of the temperature and relative humidity in Tsukuba (Japan Meteorological Agency 2019). Red and blue thin lines indicate the daily average temperature and relative humidity, respectively. Red and blue thick lines represent the weekly average temperature and relative humidity for one week before that day, respectively. In Tsukuba, it is hot and humid in the summer, and cold and dry in the winter. Comparing with the chart in

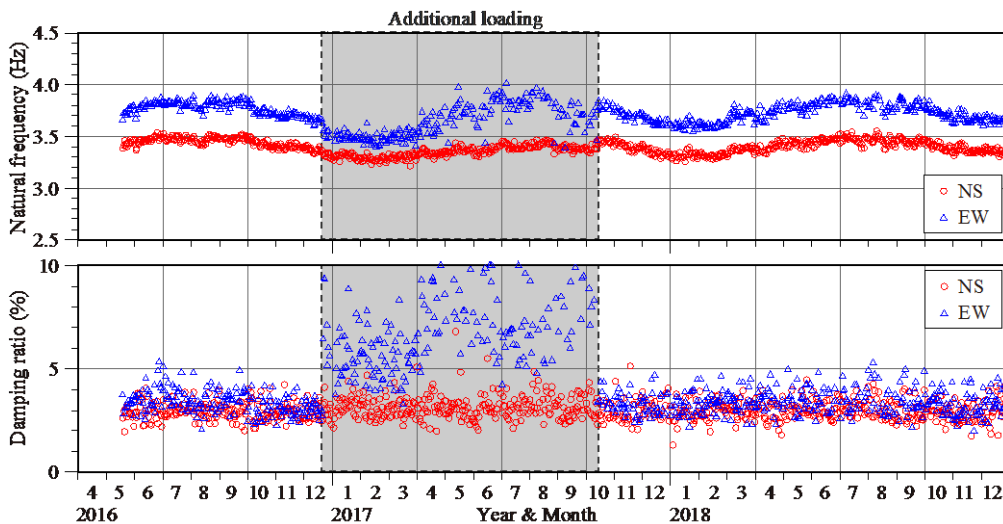


Figure 3: Changes in natural frequency and damping ratio with time, identified using ambient vibrations.

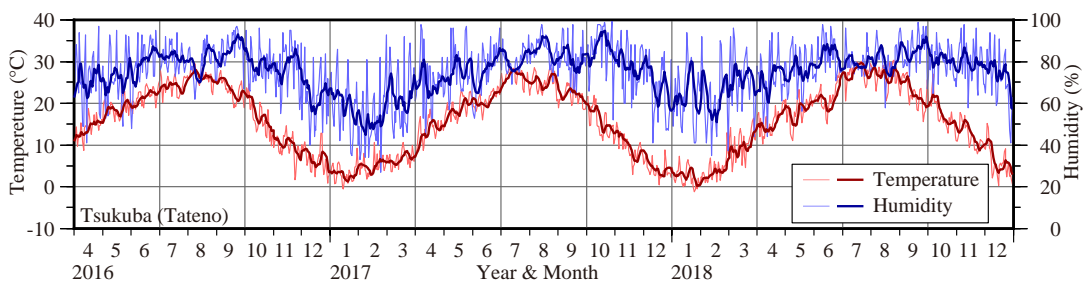


Figure 4: Daily and weekly averages of the temperature and relative humidity in Tsukuba (Japan Meteorological Agency 2019)

Figure 5, it seems that the natural frequency correlates with the temperature and relative humidity.

In order to clarify the relationship of the natural frequency to the temperature and relative humidity, multiple regression analysis is carried out. The data during the period with additional loading were eliminated in the analysis. The results of the regression analysis are shown in Equations (1) and (2).

$$f_{NS} = 3.171 + 0.00213H_W + 0.00488T_W, R^{2'} = 0.766 \quad (1)$$

$$f_{EW} = 3.424 + 0.00261H_W + 0.00692T_W, R^{2'} = 0.756 \quad (2)$$

where  $f_{NS}$  and  $f_{EW}$  are the natural frequencies (Hz) in NS and EW directions, respectively,  $H_W$  is the weekly average of relative humidity (%),  $T_W$  is the weekly average of temperature ( $^{\circ}\text{C}$ ), and  $R^{2'}$  is the adjusted coefficient of determination.

The values  $R^{2'}$  exceed 0.75 in both the directions, therefore it can be regarded that the regression models are generally significant.

To remove the influence of the temperature and relative humidity, the daily natural frequencies are converted to the values corresponding to the temperature of  $15^{\circ}\text{C}$  and relative humidity of 75% using the regression results. The converted natural frequencies are plotted in Figure 5. The seasonal fluctuations of the natural frequencies were almost eliminated and the changes in the natural frequencies during the period with the additional loading were clarified.

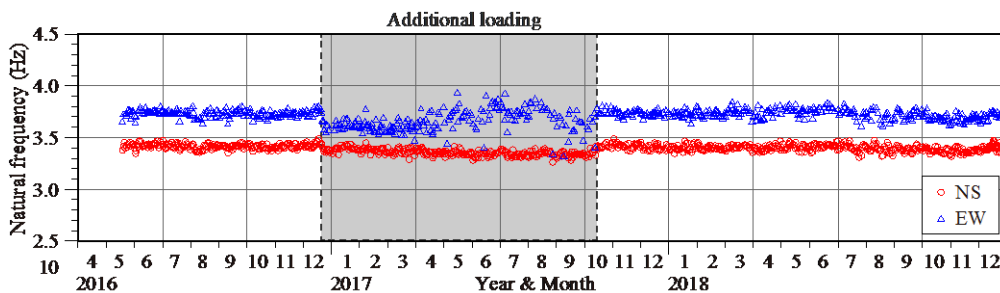


Figure 5: Changes in converted natural frequency corresponding to the temperature of  $15^{\circ}\text{C}$  and relative humidity of 75%.

## 5 DYNAMIC CHARACTERISTICS OF THE BUILDING

### 5.1 Change in dynamic characteristics with time

Since the observation was begun, strong motion data of more than 100 earthquakes have been recorded until December 2018. From each strong motion data, the fundamental natural frequencies and damping ratios in two horizontal directions of the building were identified using a parameter optimization technique (Kashima et al. 2014). With a single-degree-of-freedom system, the natural frequency and damping ratio that had the most fitted response displacement were determined using the grid search. Strong motion data recorded by the sensor on the first floor was adopted as the input motion to the system. The identified frequencies were converted to the values corresponding to the temperature of  $15^{\circ}\text{C}$  and relative humidity of 75% as well.

Figure 8 indicates changes in natural frequency and damping ratio of the experimental building with time. Red hollow circles ( $\circ$ ) and blue hollow triangles ( $\Delta$ ) correspond to the NS and EW directions, respectively. Looking at the upper plot, fluctuations in natural frequency are quite large in both the directions. The natural frequencies in the NS directions are distributed between 3.0 and 3.7 Hz, and those in the EW directions between 3.5 and 4.1 Hz. Although the damping ratios in both the directions vary widely as well, those are generally distributed between 2% and 4% except during the period with the additional loading.

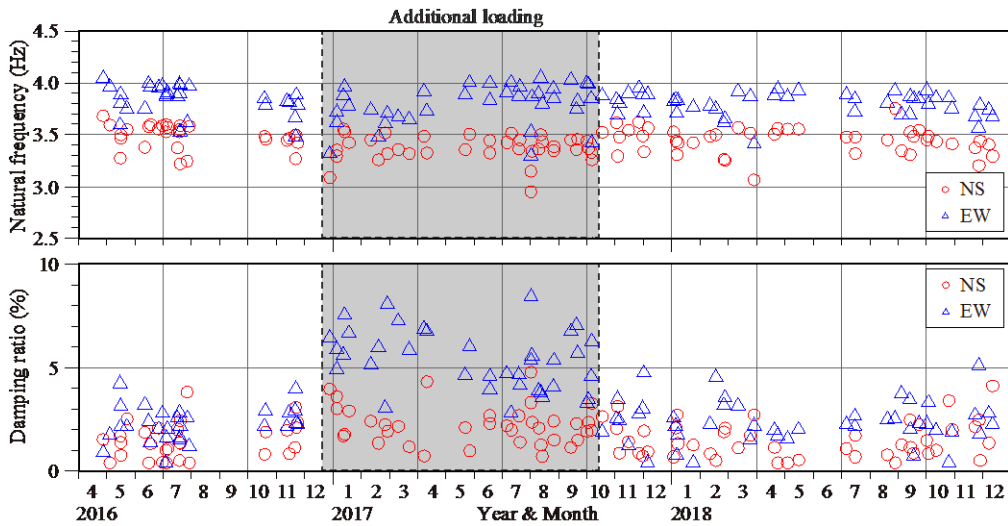


Figure 6: Changes in converted natural frequency and damping ratio with time, identified using strong motion data.

## 5.2 Amplitude-dependence of dynamic characteristics

In order to examine the amplitude-dependence of the dynamic characteristics, the maximum displacement angle  $\theta_{max}$  is adopted to represent the seismic response amplitude.

$$\theta_{max} = |x_T(t) - x_F(t)|_{max}/H \quad (3)$$

where,  $x_T(t)$  and  $x_F(t)$  are the time histories of the displacements on the sixth and first floors, respectively, and  $H$  is the height of the sixth-floor level from the first-floor level.

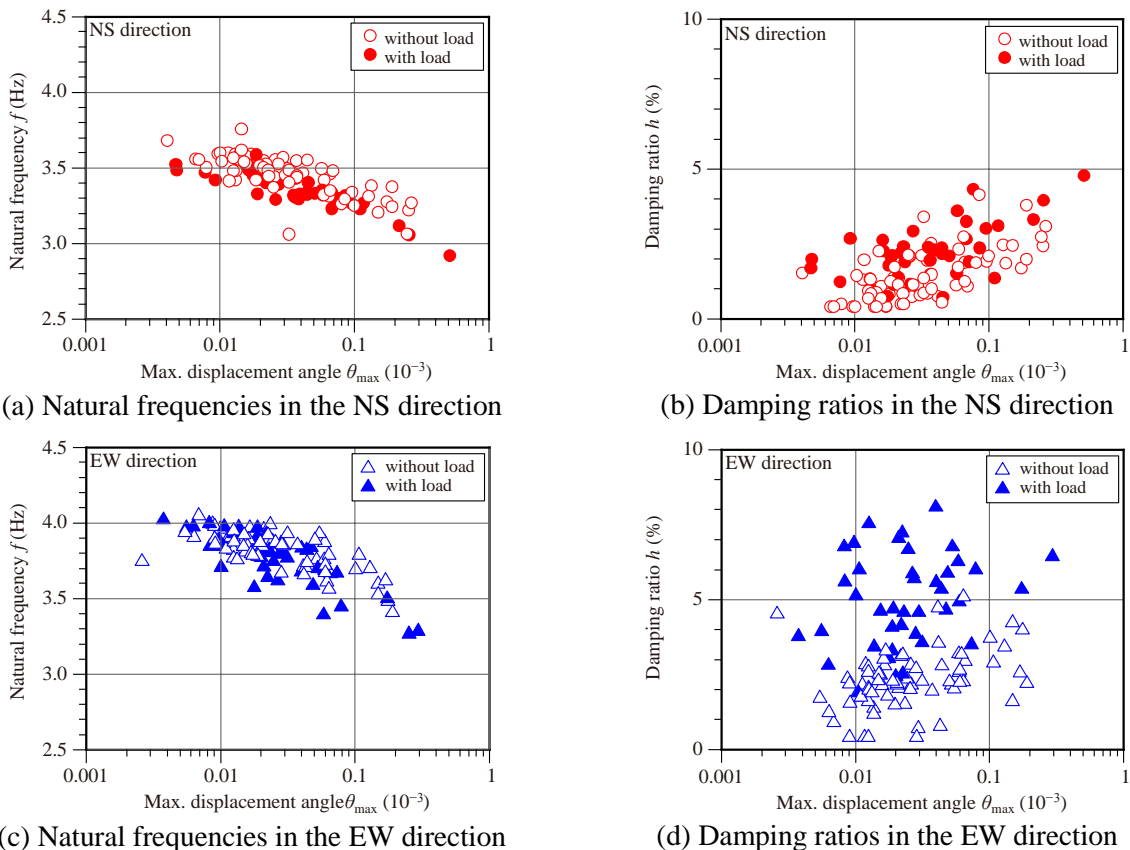


Figure 7: Relation of the converted natural frequency and damping ratio to max. displacement angle  $\theta_{max}$

The relation of the natural frequency and damping ratio to the maximum displacement angle  $\theta_{\max}$  is plotted in Figure 9. The natural frequencies and damping ratios in the NS direction are plotted in (a) and (b), and those in the EW direction in (c) and (d). In all the plots, hollow ( $\circ$  and  $\triangle$ ) and solid ( $\bullet$  and  $\blacktriangle$ ) symbols indicate values obtained during the time periods without and with the additional loading, respectively. In both the directions, the natural frequencies become lower as the maximum displacement angles increase. Comparing the natural frequencies between the cases without and with the additional loading, it seems that the natural frequencies with the additional loading are lower than those without the additional loading in the NS direction. In contrast, the damping ratios become larger as the maximum displacement angles increase. The reason that the damping ratios during the period with additional loading are large is the effect of the sloshing of the water pools, as mentioned above.

## 6 CONCLUSIONS

We minutely discussed the dynamic characteristics of the six-storey wooden experimental building using strong motion data and ambient vibration data. The result can be summarised as follows;

The natural frequencies of the system with swaying and rocking in the NS and EW directions were identified as 3.02 Hz and 3.22 Hz, respectively, through the analysis using a set of strong motion data. The natural frequencies of the system with rocking are about 10% higher than those values. In the vibration mode shapes estimated from the strong motion data, the ratios of the swaying and rocking displacements to the top displacement in the NS component are about 7% and 25 %, respectively. Those in the EW component are about 7% and 18%.

Seasonal fluctuation in the natural frequencies could be observed through the system identification using ambient vibration data. This could be explained as the influence of the temperature and relative humidity.

The natural frequencies and damping ratios identified from the strong motion data have some variations. The dependence of the dynamic characteristics on amplitude is essential one of the causes of the variation. The natural frequencies become lower as the maximum displacement angles increase in both the directions. The damping ratios in both the directions seem to elevate with the increase in maximum displacement angle.

## 7 ACKNOWLEDGEMENTS

We express our gratitude to Mr. Tsujimura and Ms. Fukuba, former staff members of the Japan 2x4 Builders Association, for their considerable cooperation. Some figures are plotted using Generic Mapping Tools (GMT) (Wessel et al. 2013). The authors thank them for providing such excellent software.

## 8 REFERENCES

- Japan Meteorological Agency. 2019. <https://www.jma.go.jp/>.
- Kashima, T. & Nakagawa H. 2018. Strong Motion Instrumentation in a Six-story Wooden Building and Analysis of Its Dynamic Characteristics, *16th European Conference on Earthquake Engineering (16ECEE), Thessaloniki, 18-21 June 2018*. Paper # 10192.
- Stewart, J.P., Seed, R.B. & Fenves. 1998. *Empirical Evaluation of Inertial Soil-Structure Interaction Effects*, Report No. PEER-98/07, Pacific Earthquake Engineering Research Center, University of California, Berkeley
- Tamura, Y., Sasaki A. & Tsukagoshi, H. 1993. Evaluation of Damping Ratios of Randomly Excited Buildings using the Random Decrement Technique, *Journal of Structural and Construction Engineering*, Architectural Institute of Japan, Vol 454 29-38 (in Japanese).
- Tsujimura, Y. 2016. Report on a 6-storey Wood-frame Structure Experimental Building Project, *Wood Industry*, Wood Technological Association of Japan, Vol 71(8) 329-332 (in Japanese).
- Wessel, P., Smith W.H.F., Scharroo R., Luis J. & Wobbe F. 2013. Generic Mapping Tools: Improved version released, *EOS Trans. AGU*, Vol 94 409-410.